RSC Advances

PAPER

View Article Online
View Journal | View Issue

Check for updates

Cite this: *RSC Adv.*, 2020, **10**, 18339

Self assembled monolayer of silica nanoparticles with improved order by drop casting†

Asma Qdemat, *[ab] Emmanuel Kentzinger, [a] Johan Buitenhuis, [c] Ulrich Rücker, [a] Marina Ganeva [d] and Thomas Brückel [ab]

This paper reports on the formation of large area, self assembled, highly ordered monolayers of stearyl alcohol grafted silica nanospheres of ≈50 nm diameter on a silicon substrate based on the drop-casting method. Our novel approach to achieve improved order uses stearyl alcohol as an assistant by adding it to the colloidal NanoParticle (NP) dispersion from which the monolayers are formed. Additionally, a heat treatment step is added, to melt the stearyl alcohol in the monolayer and thereby give the particles more time to further self-assemble, leading to additional improvement in the monolayer quality. The formation of the monolayers is significantly affected by the concentration of the NPs and the stearyl alcohol, the volume of the drop as well as the time of the heat treatment. A high surface coverage and uniform monolayer film of SiO_2 NPs is achieved by appropriate control of the above-mentioned preparation parameters. Structural characterization of the obtained SiO_2 NP monolayer was done locally by Scanning Electron Microscopy (SEM), and globally by X-ray reflectivity (XRR) and grazing incidence small-angle X-ray scattering (GISAXS), where the data was reproduced by simulation within the Distorted Wave Born Approximation (DWBA). In conclusion, our modified drop-casting method is a simple, inexpensive method, which provides highly ordered self-assembled monolayers of silica particles, if combined with a compatible additive and a heat treatment step. This method might be more general and also applicable to different particles after finding an appropriate additive.

Received 31st January 2020
Accepted 29th April 2020

DOI: 10.1039/d0ra00936a

rsc.li/rsc-advances

Open Access Article. Published on 13 May 2020. Downloaded on 2/12/2026 7:44:12 PM.
This article is licensed under a Creative Commons Attribution-NonCommercial 3.0 Unported Licence.

Introduction

Assembly of NPs into large-area monolayers on a solid substrate is fundamentally interesting due to their unique optical and electronic properties. Furthermore, they have an impact on the creation of next-generation materials design[1] and for new devices that require monolayers with ordered structure over large areas formed with a simple method at low cost to meet the growing industrial needs. But controlling the deposition on a substrate to obtain two-dimensional and three-dimensional nanoparticle arrays is a complex process, and it occurs under specific conditions.

Several methods for fabricating highly ordered monolayers of NPs on solid substrates have been reported, such as electron beam lithography,[2] dip coating,[3] spin coating,[4,5] Langmuir–Blodgett (LB) technique[6] and capillary immersion force technique.[7] Y. Wang demonstrated highly ordered and closely packed, self assembled monolayers of microsized SiO_2 spheres on a silicon substrate and on a glass substrate by the dip coating method[8] and Ogi *et al.*[4] report the fabrication of a monolayer of SiO_2 nanoparticles of size 550 and 300 nm on sapphire substrates by using the spin coating method.

The above methods typically result in small monolayer areas and non-uniformity of the resulting monolayer. Due to these disadvantages, these methods are not suitable for industrial processes. Drop-casting is a simple, cheap method and permits the formation of a monolayer over a large area. Due to these advantages, the drop-casting method has potential for industrial applications.

In this paper, we report on the fabrication of a large-area monolayer of SiO_2 NPs (≈50 nm in diameter) with a high surface coverage on top of a silicon substrate using a drop-casting method. However, the monolayers formed in this way have a lot of cracks between small ordered domains. Therefore, we improve the quality of the monolayers by adding some stearyl alcohol to the NP dispersions, to try to fill all gaps between the NPs in the monolayers formed early in the drying stage, and thereby preventing crack formation. Finally, we further improve the monolayer quality by adding an additional heat treatment step. We find that high-quality monolayers can

[a]*Jülich Centre for Neutron Science, Peter Grünberg Institute, JARA-FIT, Forschungszentrum Jülich GmbH, 52425 Jülich, Germany*
[b]*RWTH Aachen, Lehrstuhl für Experimentalphysik IVc, Jülich-Aachen Research Alliance (JARA-FIT), 52074 Aachen, Germany*
[c]*Biomacromolecular Systems and Processes, IBI-4, Forschungszentrum Jülich GmbH, 52425 Jülich, Germany*
[d]*Forschungszentrum Jülich GmbH, Jülich Center for Neutron Science at MLZ, Lichtenberg Straße 1, 85748 Garching, Germany*

† Electronic supplementary information (ESI) available. See DOI: 10.1039/d0ra00936a

Open Access Article. Published on 13 May 2020. Downloaded on 2/12/2026 7:44:12 PM.
This article is licensed under a Creative Commons Attribution-NonCommercial 3.0 Unported Licence.

be obtained by using a suitable concentration of the NP and stearyl alcohol, proper drop volume and optimizing the heating time.

The silica nanoparticles used in the present study have two important advantages. First of all, they can be prepared with a narrow size distribution (<4%) which is essential for the self-assembly process. Second, the surface of the particles can be chemically modified resulting in particles, which, if dried carefully, do not immediately aggregate irreversibly, which might increase the time for self-assembly. In addition, the relatively low Hamaker constant of silica as compared to other inorganic materials, limits the van der Waals attraction between the cores of the particles, making them more free to move, thereby favoring self-assembly to high-quality monolayers. Generally, the possibilities for chemical modification of the surface of silica particles as well as within the particles, has led to their use in various fields such as medicine, biology, engineering and the development of customized materials.[9]

Experimental

N-type Si (100) wafers, 0.5 mm thick, cut into 10 × 10 mm^2 pieces were used as a substrate for NP deposition, and were cleaned as follows before deposition. The Si substrates were alternately ultra-sonicated in acetone, ethanol, and deionized (DI) water for 5 min, respectively. After that, the wafers were stored in ethanol. Nitrogen gas was used to dry the Si substrates directly after taking them out of the ethanol, just before NPs deposition. This procedure was used to remove dust particles and contamination from the substrate surface. After the above treatment, the drop-casting method was used to deposit NPs on the substrates as explained in detail later.

Monodisperse silica particles were prepared in two steps. First monodisperse core silica particles were synthesized in a reverse microemulsion system.[10–12] After purification from the microemulsion, the particles were grafted with stearyl alcohol following van Helden.[13] In this procedure, the stearyl alcohol forms covalent bonds to the silica surface, resulting in a quite dense stearyl alcohol layer[13,14] of about 2 nm thickness, as demonstrated by carbon content analysis on several stearyl grafted silica particles of different sizes.[13] In addition, this was also confirmed by a small angle neutron scattering contrast variation study[14] for stearyl silica particles dispersed in toluene, which were very similar to the present ones, only the present ones are more monodisperse. This gives sterically stabilized colloidal silica nanoparticles, which can be dispersed in nonpolar solvents like cyclohexane, chloroform or toluene. Here particles with a diameter of about 50 nm were obtained, using toluene as a solvent. The statistical particle size and size distribution of the synthesized silica nanospheres have been determined by several methods (see ESI† for details). Concentrations are expressed as volume fractions, which are calculated using the densities of solvent, silica and stearyl alcohol and assuming additivity of volumes. For the stearyl alcohol silica particles an average density of 1.8 g mL^{-1} was used, which is also in agreement with a density measurement on former stearyl alcohol silica colloids of similar size. A colloidal dispersion with 5.4 vol% stearyl alcohol silica nanoparticles was prepared as stock. In addition, a stock solution of 5.4 vol% stearyl alcohol in toluene was made.

These two stock solutions were used to fabricate a large monolayer area of ordered nanoparticles on a silicon substrate by the drop-casting technique with and without the assistance of stearyl alcohol. The monolayer preparation methods were carried out as follows. Method 1: prior to the use of stearyl alcohol to assist monolayer formation, ≈5 μL of 5.4 vol% NPs stock dispersion was dropped onto a cleaned silicon substrate, followed after one minute by the addition of an extra ≈3 μL toluene to the film. While doing so, the sample was kept unmoved and the sample container was covered to reduce the evaporation rate. Method 2: in order to improve the NPs ordering over the whole sample area, stearyl alcohol was used as assistant. Firstly, in this method, a solution with 0.1 vol% stearyl alcohol silica and 0.1 vol% stearyl alcohol was prepared, by adding 20 μL of 5.4 vol% stearyl alcohol silica and 20 μL of 5.4 vol% stearyl alcohol to 0.96 mL of toluene. After that, 5 μL of this solution was taken by a micro-pipette and dropped onto the silicon substrate. Then the droplet quickly spreads over the substrate surface and the sample was left open for one day to let it dry. Method 3: a last optional step added in the monolayer fabrication is the heat treatment, which was used in order to reduce the number of cracks in the monolayer obtained in method 2.

Characterization of SiO_2 NP monolayers has been done by scanning electron microscope (SEM, Hitachi SU8000) to image the ordering of the NPs locally in real space. In addition, XRR and GISAXS measurements were carried out at the diffractometer Gallium Anode Low-Angle X-ray Instrument GALAXI[15] using a monochromatic X-ray beam with a wavelength of $\lambda = 0.1314$ nm and a beam of a cross-section at the sample of 0.7 × 0.7 mm^2. XRR measurements were performed in order to obtain the depth resolved profile of the NPs in reciprocal space. GISAXS measurements were performed in order to investigate the in-plane ordering of the NPs. In GISAXS, the X-rays are incident on the sample at a grazing angle α_i, and the scattering pattern is recorded by a Pilatus 1M 2D position-sensitive detector with 169 × 179 mm^2 active area at a sample-detector distance of 3528 mm.

Formation of NP monolayers and local characterization by SEM

Method 1: nanoparticles monolayer by simple drop casting. Fig. 1 shows SEM images at different locations and under various magnifications of the SiO_2 NP monolayers obtained by method 1: simple drop casting with and without adding additional toluene and reducing its evaporation rate by covering the sample as described before. Although the evaporation rate could be expected to affect monolayer formation,[16] adding additional toluene and reducing the evaporation rate by simply covering the sample did not make a significant difference, maybe because the evaporation rate of toluene remains fast with and without these additional simple measures. From the images, it is seen that the particles do not cover the whole surface area of the substrate. There are some areas covered with

 This journal is © The Royal Society of Chemistry 2020

Open Access Article. Published on 13 May 2020. Downloaded on 2/12/2026 7:44:12 PM.
This article is licensed under a Creative Commons Attribution-NonCommercial 3.0 Unported Licence.

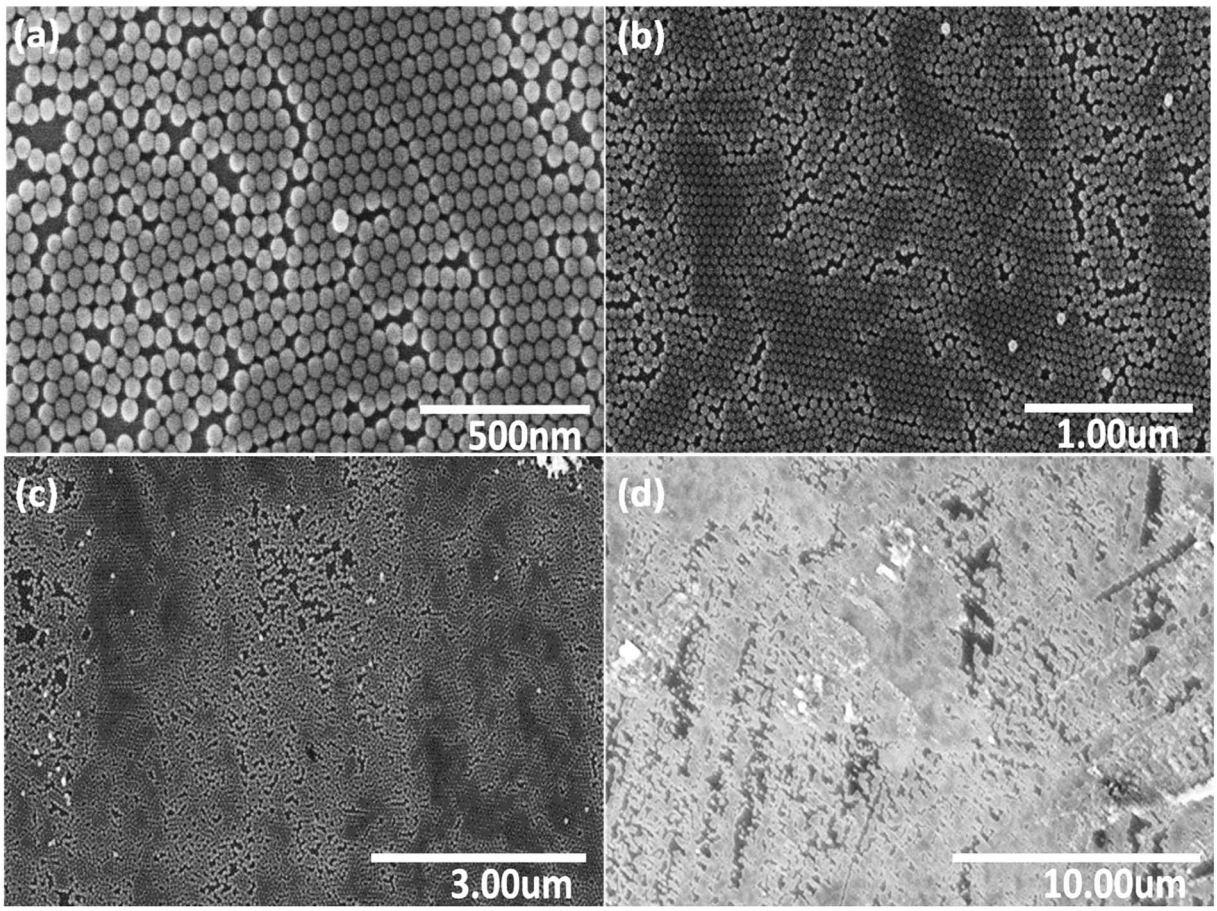

Fig. 1 Series of SEM images (a)–(d) with various magnifications, taken at different positions of a monolayer of SiO_2 NPs, assembled on a silicon wafer with extra toluene added after drop casting (without stearyl alcohol).

only a few NPs and some areas, where particles can be found above the first layer. Also, over some areas, the particles are randomly and irregularly distributed. The same results are observed for a monolayer of SiO_2 NPs, assembled on a silicon wafer without extra addition of toluene (without stearyl alcohol) as shown in the SEM image (Fig. S2) in the ESI.† The monolayer produced by this method is usually not homogeneous over large sample areas, which might be due to the surface tension leading to a contraction of the particle grains during drying of the sample. Nevertheless, with the present monodisperse particles with a small size distribution of <4% as used, some areas with a reasonable degree of ordering are obtained.

Method 2: improved monolayer quality by stearyl alcohol assistance. The monolayers obtained by the simple drop-casting method show several defects. The ordered domains are small and separated by cracks and in addition some tendency to multilayer formation is observed. Referring to the origin of the cracks, we considered the following explanation. After drop-casting, a thin film of colloidal dispersion of NPs is formed, which (partially) self-assemble and at the same time starts to dry. During this process it might be that monolayers of better quality could form by self-assembly, when the particles are still free to move. Then, on further drying, the coherent contraction of the monolayer dimensions is opposed by pinning of domain edges to substrate surfaces at the late stages of drying, *i.e.* the NPs become less free to move, which then eventually might lead to cracks. Therefore, it was considered that adding stearyl alcohol might fill the gaps between the particles in the monolayer and thereby reduce crack formation.

In the experiments, the influence of the volume of the droplet, the concentration of silica particles and the stearyl alcohol on the surface coverage and the uniformity of the monolayer on the wafer were investigated. Here, we considered a 5 μL droplet with 0.1 vol% NPs and 0.1 vol% stearyl alcohol to be the suitable parameters to improve the monolayer quality. When an excessively high concentration and large droplet volume is used, multilayers of silica particles are formed. While, at low concentration and small droplet volume, only separated islands are formed. More details about the preparation of the colloidal dispersion and its mixture with stearyl alcohol are given in Section 2.

Fig. 2 shows a series of SEM images at different locations and under various magnifications of the NP monolayer obtained after using stearyl alcohol as assistant. As can be seen from the SEM images, less particles are observed in a second (or third) layer, *i.e.* less multi-layer formation is observed. However, still a lot of cracks appear in the resulting monolayers. So unfortunately, our idea to reduce crack formation by the sole addition

Open Access Article. Published on 13 May 2020. Downloaded on 2/12/2026 7:44:12 PM.
This article is licensed under a Creative Commons Attribution-NonCommercial 3.0 Unported Licence.

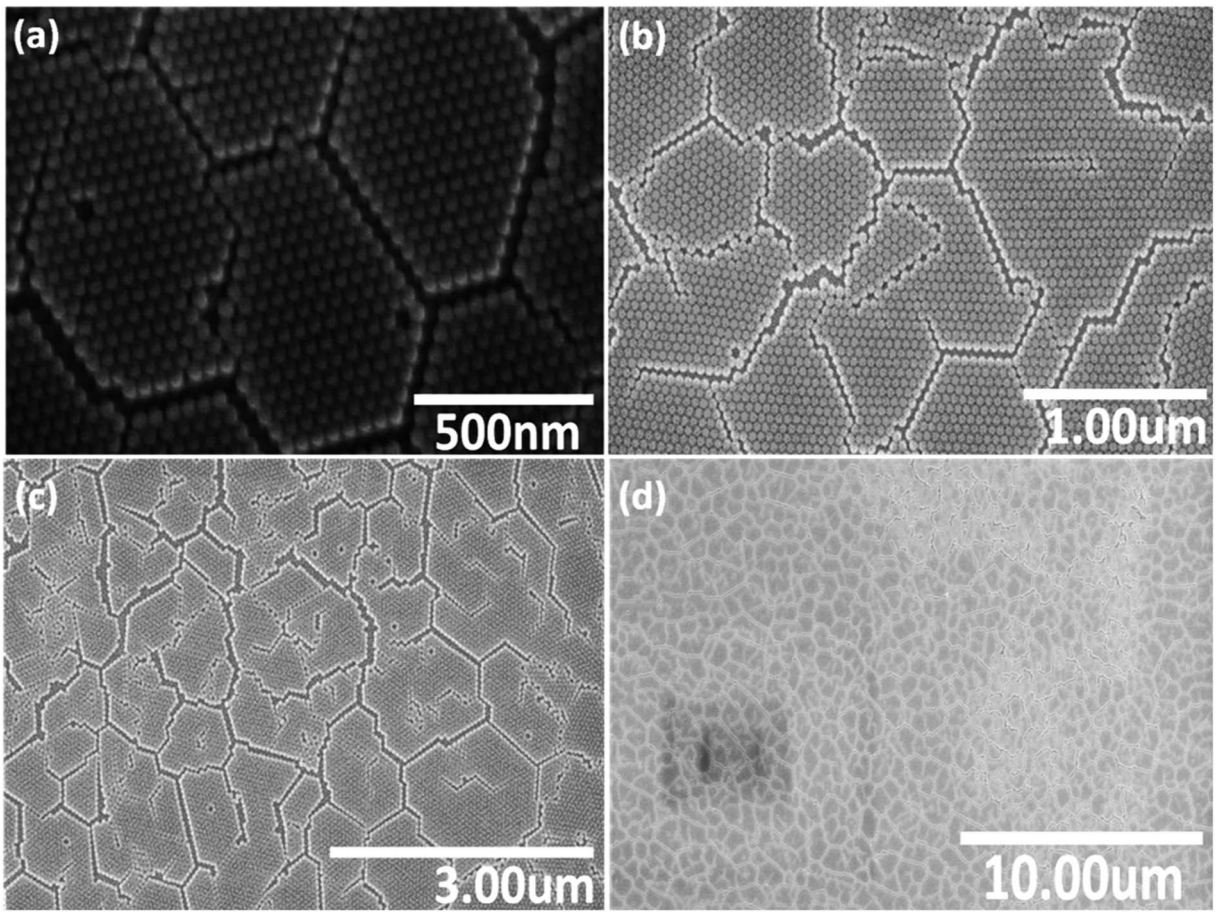

Fig. 2 Series of SEM images (a)–(d) with various magnifications, taken at different positions of a monolayer of SiO_2 NPs, assembled on a silicon wafer after using stearyl alcohol as assistant.

of stearyl alcohol does not work. However, the monolayers formed are more long range ordered, *i.e.* many hexagonal domains which are separated by cracks, still have the same orientation. So the monolayers obtained by the addition of stearyl alcohol are significantly better compared to the monolayers obtained by the simple drop-casting method.

The reason for the resulting large monolayer is not clear as the effect of the stearyl alcohol is complex. For instance, the precipitation of the stearyl alcohol on evaporation of the toluene, might first take place on the particles and/or on the surface of the wafer. Moreover, the continuous evaporation of the toluene and possible drying from the edge of the droplet, might also play a key role on the monolayer formation. However, this is very speculative and work on the mechanism of this monolayer formation is not easy[17] and outside the scope of the present study.

Method 3: improved nanoparticle ordering *via* annealing process. In order to avoid the cracks and other defects in the monolayers with stearyl alcohol from the previous paragraphs, the monolayers were heat treated in an oven. The idea was to melt the stearyl alcohol in the monolayer obtained by the previous method, thereby obtaining free mobile particles again, which are free to move and self-assemble further, to obtain a layer with improved order. After further self-assembly we can solidify the ordered layer with only a minor change in volume by simply cooling to room temperature. The essential aspect of solidifying the monolayer by freezing the stearyl alcohol as compared to simple evaporation of a solvent, was thought to be the advantage of the annealing step leading to the minor volume change. This can reduce the number of cracks, which are believed to originate from the volume change during monolayer formation by evaporation, a process which could be compared to crack formation sometimes observed in dry soil.

In order to test the idea from the previous section, the monolayer obtained in the previous section was treated at a temperature of about 70 °C, which is 10 degrees above the melting point of stearyl alcohol. The time of the heat treatment was varied in a broad range from 15 minutes up to 10 days. To prevent the slow evaporation of the small amount of stearyl alcohol in the monolayer, we put the sample in a small closed polystyrene box together with a small stearyl alcohol grain, to obtain a stearyl alcohol atmosphere. The optimal heat treatment time was found to be the longest time used of 10 days. However, maybe higher temperature can reduce this time significantly. Furthermore, for industrial requirements, lots of samples can be treated in one oven at the same time. SEM

 This journal is © The Royal Society of Chemistry 2020

Open Access Article. Published on 13 May 2020. Downloaded on 2/12/2026 7:44:12 PM.
This article is licensed under a Creative Commons Attribution-NonCommercial 3.0 Unported Licence.

images taken after different duration in the oven at 70 °C are shown in Fig. 3. As can be seen from the SEM images, the degree of ordering improves with longer time in the oven.

Especially for the sample after 10 days a large, uniform, homogeneous monolayer of SiO_2 NPs with very large correlation lengths is obtained, also with a good hexagonal order. The ordering between NPs over the whole sample area is evidently improved and the number of cracks is reduced, compared to the first simple drop-casting method without stearyl alcohol and also compared to the second method using stearyl alcohol, but without heat treatment.

Global and depth-resolved characterization by XRR and GISAXS

X-ray reflectivity. X-ray reflectometry measurements were performed to provide statistical information on the average electron density distribution with respect to the vertical axis, to reveal the out of plane ordering of the nanoparticles, to determine layer thickness and the interface roughness. Fig. 4(a)–(c) show the XRR data of the as-prepared monolayers in method 1, method 2 and method 3, respectively. Qualitative differences between the XRR curves are obvious. The reflectivity curve in Fig. 4(c) shows Kiessig fringes up to high values of the scattering vector magnitude Q which proves that a highly ordered, homogeneous and uniform monolayer of NPs over a large surface area exists. In Fig. 4(b) the Kiessig fringes observed are much less intense than in Fig. 4(c), while the Kiessig fringes in Fig. 4(a) almost vanish. The critical angle (α_c) for total reflections at $Q_z = 0.3\ nm^{-1}$ does not change for all XRR curves shown in Fig. 4. This value corresponds to the one for the silicon substrate.

The XRR curve (red point) of the monolayers with stearyl alcohol after 10 days of heat treatment is shown in Fig. 4(c) along with the fit (black solid line). As explained in Section 3.1 of the ESI,† the measured reflectivity curve is well reproduced by assuming a parabolic scattering length density profile of the NP layer. A detailed description of the data treatment is given in the ESI.†

To fit the measured XRR curve of the monolayers obtained after 10 days of heat treatment, we assumed the layer model drawn in Fig. 4(d) consisting of the particle layer on top of the silicon substrate (dark gray). The left side shows the cross section of the model and the right side shows the scattering length density (SLD) variation along the perpendicular direction to the film as extracted from the fit.

GISAXS. SEM provides a qualitative information about only a few micron squared sized areas. Therefore, GISAXS measurements were carried out to investigate a much larger

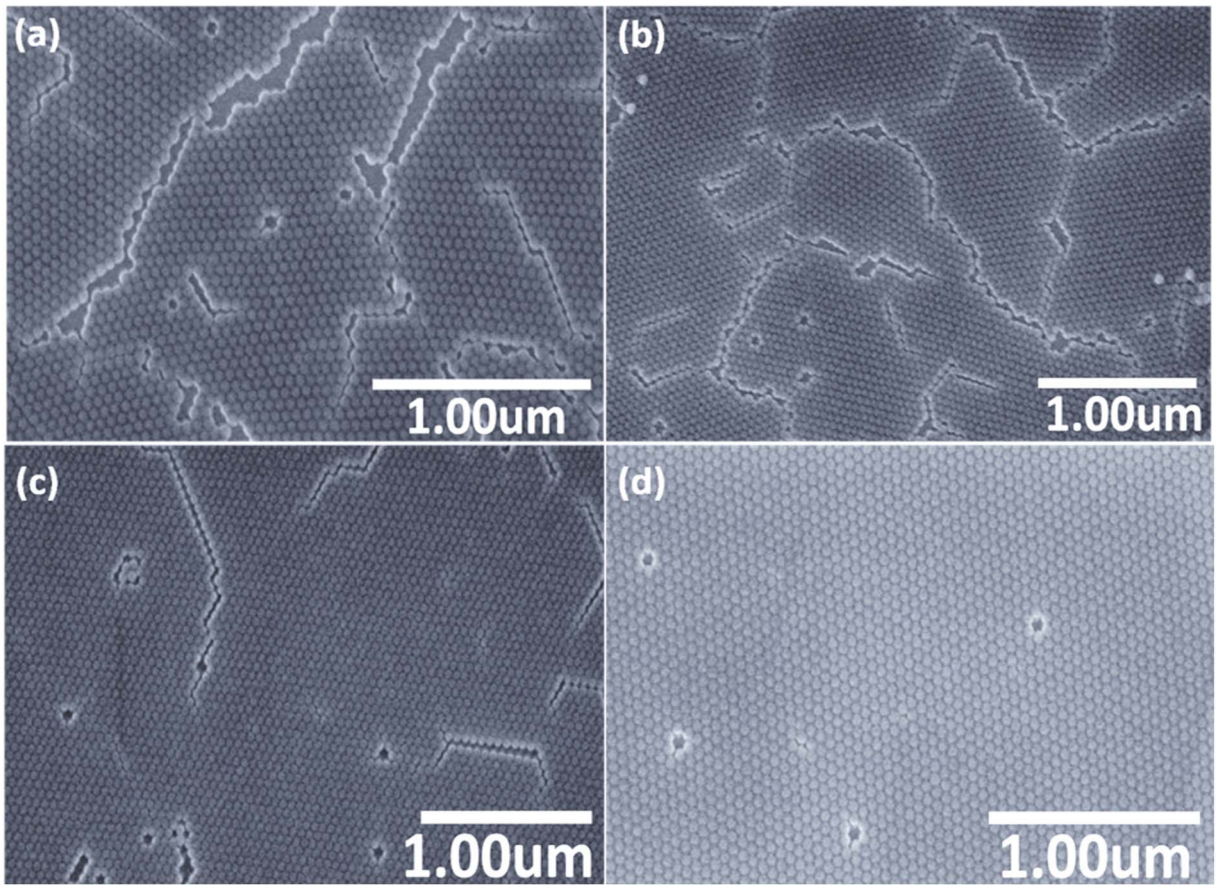

Fig. 3 SEM images of stearyl alcohol silica monolayer with stearyl alcohol as assistant on silicon substrate heated-treated at 70 °C for various period of time: (a) 15 min, (b) 2 hours, (c) 29 hours, (d) 10 days.

Open Access Article. Published on 13 May 2020. Downloaded on 2/12/2026 7:44:12 PM.
This article is licensed under a Creative Commons Attribution-NonCommercial 3.0 Unported Licence.

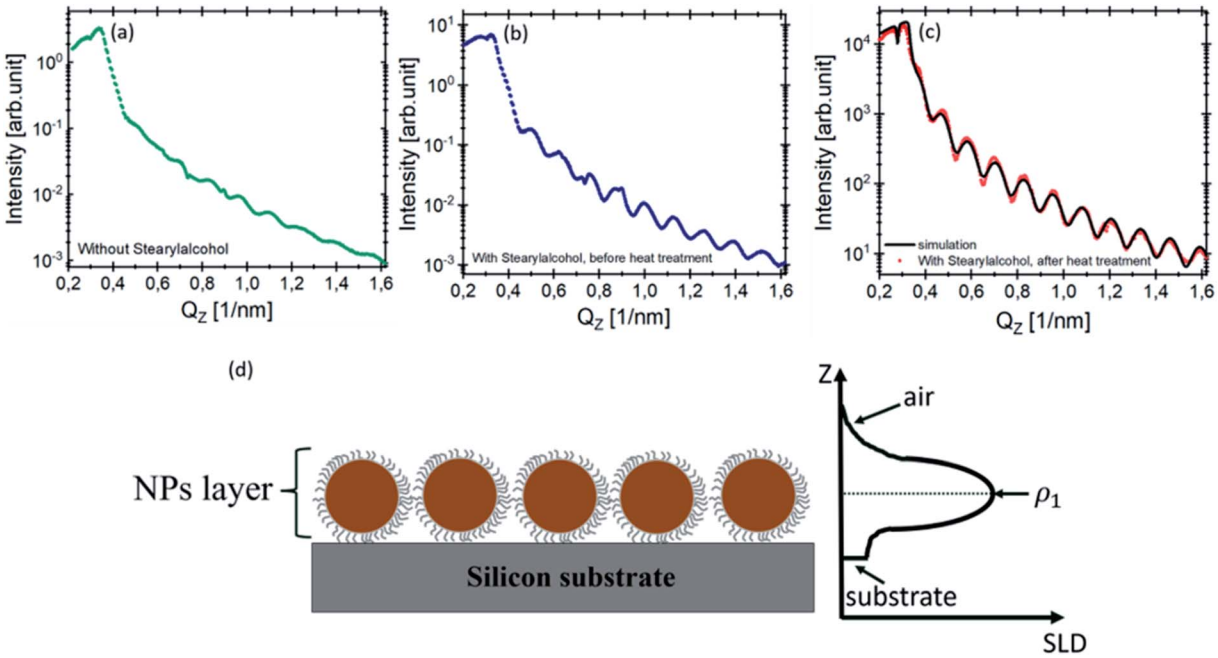

Fig. 4 X-ray reflectivity from a monolayer of SiO_2 NPs (a) without stearyl alcohol. (b) With stearyl alcohol before heat treatment. (c) With stearyl alcohol after 10 days of heat treatment (red points) along with the fit (black solid line). (d) The model layers structure assumed for fitting the data shown in (c), displaying an ideal in-plane close-packed arrangement of spherical nanoparticles with a parabolic SLD profile of the nanoparticles layer.

area of the substrate and to obtain additional information about the range of the in-plane ordering of the NPs in the monolayer. In the GISAXS measurement, a monochromatic X-ray beam with an incident wave vector $\vec{K_i}$ is directed on a sample surface with a very small incident angle α_i with respect to the surface close to the critical angle of total reflection, in order to maximize the amplitude of the X-ray wave function in sample. The X-ray is reflected off the substrate surface, scattered from the particles along $\vec{K_f}$ in the direction (α_f, θ) as illustrated in Fig. 5. More details about the geometry of GISAXS and the assignments of the axes are described in G. Renaud *et al.*[18] The periodic order of the nanoparticles in the monolayer produce a diffraction pattern of Bragg rods, which can be indexed to determine the crystal structure, the lattice constant and symmetry of the monolayer.[19,20]

Fig. 6(a)–(c) show GISAXS scattering patterns of stearyl alcohol silica monolayers on silicon substrates. The corresponding SEM images were shown previously as SEM images in Fig. 1, 2 and in 3(d), respectively. The GISAXS measurements were carried out at an incident angle of $\alpha_i \approx 0.25^\circ$. Distinct vertical Bragg rods visible in all GISAXS patterns along the Q_y direction indicate long-range periodic order of the NPs. Furthermore, the rods are sharp in Q_z direction, due to the monolayer nature of the NPs. Moreover, rings of diffuse scattering can also be observed in the GISAXS patterns, which are related to the square of the Fourier transform of the particle shape, *i.e.* the form factor of the individual NPs. Differences between the GISAXS patterns are obvious. After 10 days of heat treatment (Fig. 6(c)), the Bragg rods become more intense and sharper. Also more reflections along Q_y are visible. The appearance of these reflections is due to extended order. Furthermore, after 10 days of heat treatment (Fig. 6(c)) the diffuse rings nearly vanish compared to Fig. 6(a) and (b). This means that nearly all particles are taking part in the long range order as scattering from individual defects is largely suppressed. The intensity ratio in each GISAXS maps in Fig. 6 is quantified by comparing the integrated intensity of the Bragg

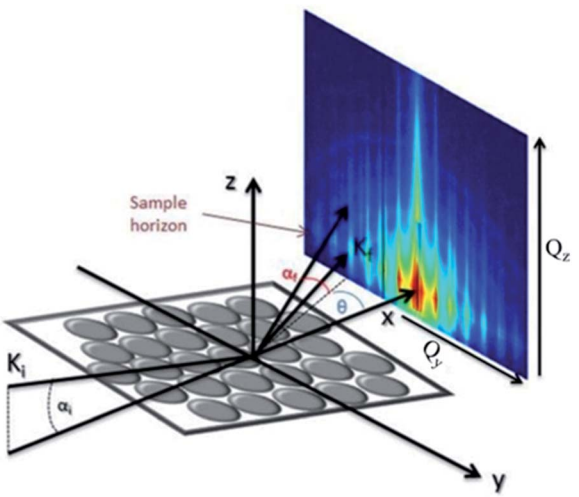

Fig. 5 Geometry of a GISAXS experiment, an X-ray beam with an incident wave vector $\vec{K_i}$, at an incident angle of α_i reflects off the substrate surface, scattering from the particles. The 2-D detector image is given in dependence on the coordination Q_y and Q_z (components of the scattering vector $\vec{Q} = \vec{K_f} - \vec{K_i}$).

This journal is © The Royal Society of Chemistry 2020

Open Access Article. Published on 13 May 2020. Downloaded on 2/12/2026 7:44:12 PM.
This article is licensed under a Creative Commons Attribution-NonCommercial 3.0 Unported Licence.

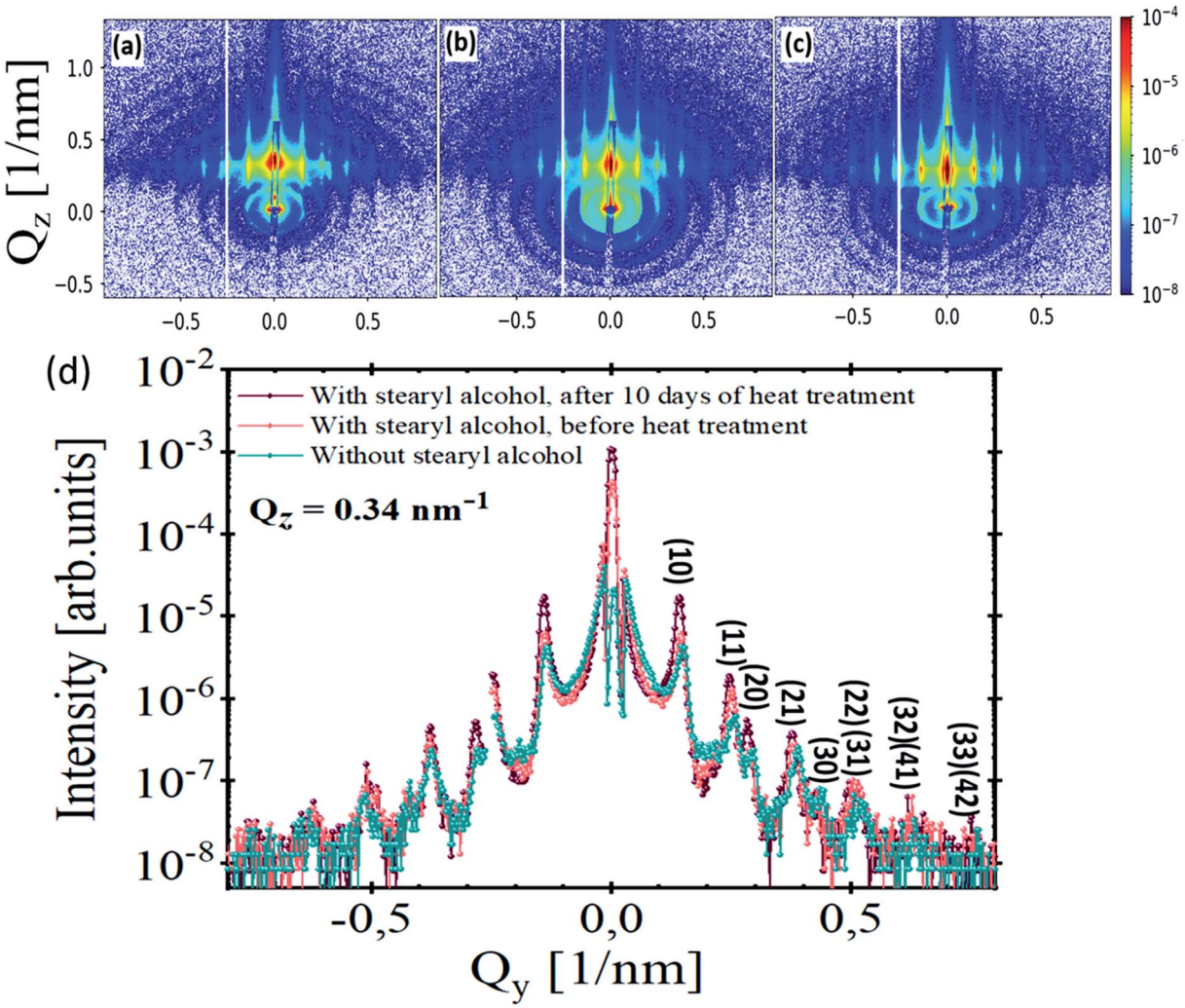

Fig. 6 GISAXS pattern of a monolayer of SiO_2 NPs deposited on silicon substrates (a) before using stearyl alcohol (b) after using stearyl alcohol, before heat treatment and (c) after 10 days heat treatment. (d) Line-cuts from (a), (b) and (c) along Q_y at a constant. $Q_z = 0.34$ nm^{-1}. The Bragg peaks are indexed by assuming a 2-D hexagonal lattice with a lattice constant $a = 51.6 \pm 0.4$ nm.

rods to the integrated intensity of the diffuse rings as explained in Section 3.2 of the ESI.† The intensity ratios for each sample are tabulated in Table 1, fourth column.

The Bragg peaks observed in the GISAXS pattern are indexed by considering a 2-D hexagonal lattice with a lattice constant $a = 51.5 \pm 0.4$ nm (value for method 3), which is larger than the particle diameter due to the stearyl alcohol molecule around the nanoparticles. The lattice constant was calculated from the (10) peak position by using the equation linking the interplanar distance d and the lattice constant a.[21] The lattice constant approximately kept the same in all samples produced from the three methods as tabulated in Table 1, second column. The line cuts from the GISAXS patterns (Fig. 6(a)–(c)) along Q_y at constant $Q_z = 0.34$ nm^{-1} are shown in Fig. 6(d). It is obvious that the Bragg peaks become more intense and sharper after 10 days of heat treatment (violet line, Fig. 6(d)). This is indicative for a larger coherence length of the crystalline structure and well-ordered NPs monolayer. After taking the instrument resolution into account, a Lorentzian profile is used to fit the first-order peak in each GISAXS pattern, which yields a structural coherence length ζ of 266 ± 2 nm, 314 ± 4 nm and >480 nm‡ for monolayers without stearyl alcohol, monolayers with stearyl alcohol before heat treatment and for monolayers with stearyl alcohol after 10 days of heat treatment, respectively.

Table 1 Lattice constant (a), coherence length (ζ) of each GISAXS map and the integrated intensity ratio between the GISAXS peaks and the diffuse rings from single defects

Method number	a (nm)	ζ (nm)	Intensity ratio
Method 1	49 ± 1	266 ± 2	2.4
Method 2	50.3 ± 0.7	314 ± 4	7.5
Method 3	51.5 ± 0.4	>480	5130

‡ About 500 nm is the resolution limit of the instrument. With the present setup only this value can be given as lower bound of the coherence length for method 3.

Open Access Article. Published on 13 May 2020. Downloaded on 2/12/2026 7:44:12 PM.
This article is licensed under a Creative Commons Attribution-NonCommercial 3.0 Unported Licence.

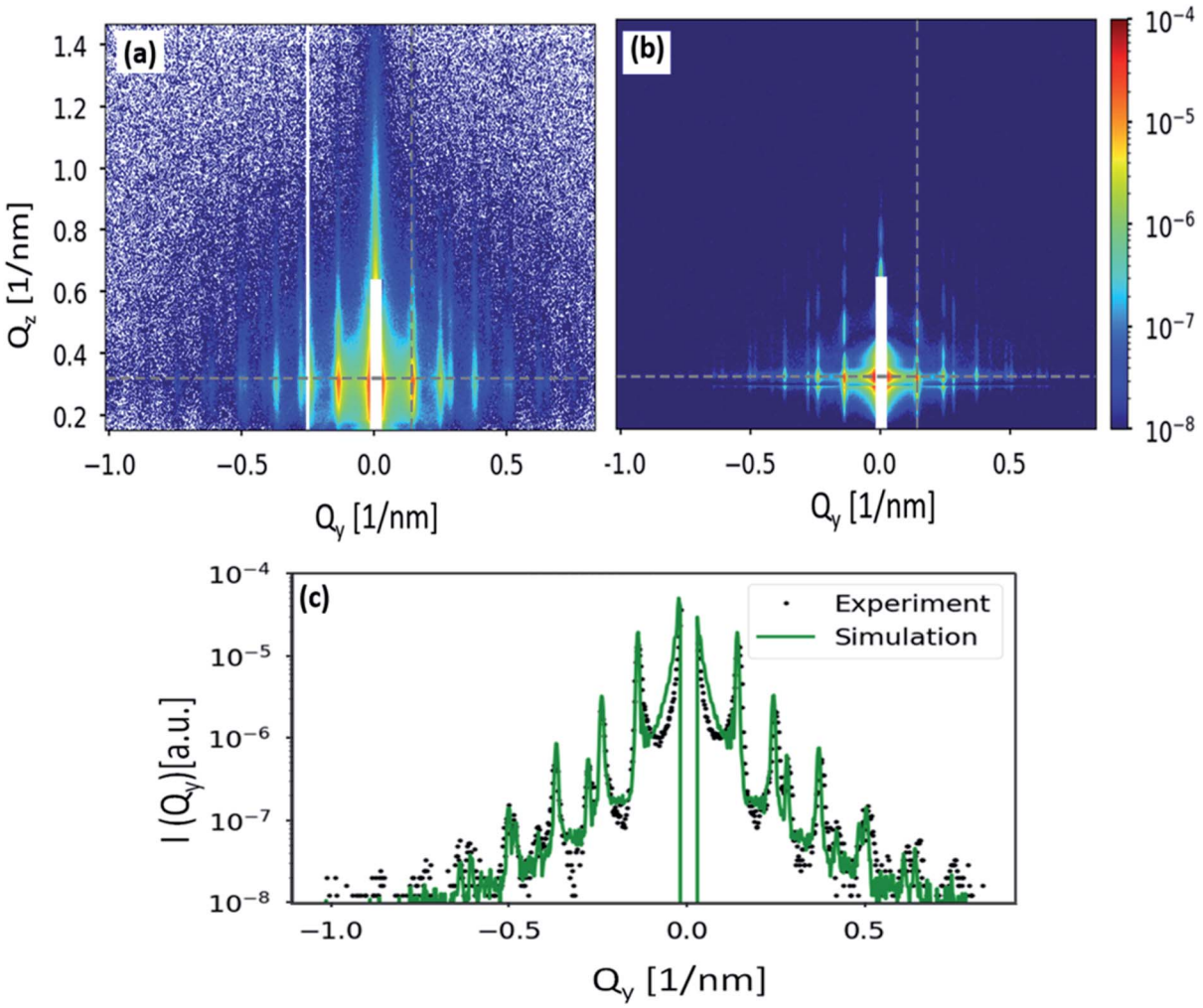

Fig. 7 (a) GISAXS pattern of SiO_2 monolayer drop-casted onto silicon substrate with stearyl alcohol after 10 days of heat treatment. (b) Simulation of the GISAXS data using BornAgain software assuming paracrystalline hexagonal lattice interference function with a lattice constant $a = 52$ nm and a spherical particle with radius of 25.5 nm. (c) A horizontal slice as a function of Q_y at $Q_z = 0.32$ nm^{-1}. The experimental data shown as black dots and the simulated data shown as a green solid line.

Finally, the GISAXS pattern in Fig. 6(c) is simulated using the BornAgain software[22] and compared with the obtained experimental result. As one can see, the simulated pattern shown in Fig. 7(b) closely reproduces the experimental data shown in Fig. 7(a). The GISAXS data has been simulated assuming a two-layers model, consists of a silicon substrate followed by the particles layer. Nanoparticles have a form factor of full sphere with SiO_2 core of 23.5 nm radius and a stearyl alcohol shell of 1.7 nm thickness. Since nanoparticles are densely packed, the ambient layer, where the NPs are situated, has been described as a graded interface. A finite 2D hexagonal lattices of randomly selected sizes have been simulated because the sample is not uniformly covered with the NPs but consists of ordered domains of variable size rotated with respect to each other. To consider the polycrystallinity of the film, an orientational distribution has been applied to the simulated domains. Positions and relative intensities of the Bragg rods (Fig. 7(a)) indicate the absence of preferred domain orientations. Therefore, a uniform orientational distribution, *i.e.* 120 lattice rotation angles in the range between 0° and 60° with equal weights, has been simulated. To account for the nanoparticles size distribution which contributes to diffuse scattering in the GISAXS pattern and broadens the structural peaks, a Gaussian size distribution with FWHM of 3 nm has been applied in the GISAXS model. A full description of the simulation is given in Section 3.3 of the ESI.† The comparison of simulated and measured GISAXS patterns is presented in Fig. 7:

(a) shows the region of interest of the measured pattern.

(b) shows the simulated pattern in the same Q range. Poisson noise has been applied to the scattering intensity.

(c) slice along Q_z at $Q_y = 0.14$ nm^{-1} (position of the first Bragg rod, shown with the vertical gray dashed line in the figures (a) and (b)).

Conclusions

In summary, we have presented a simple, inexpensive approach to obtain highly ordered self-assembled monolayers of stearyl

 This journal is © The Royal Society of Chemistry 2020

Open Access Article. Published on 13 May 2020. Downloaded on 2/12/2026 7:44:12 PM.
This article is licensed under a Creative Commons Attribution-NonCommercial 3.0 Unported Licence.

alcohol grafted silica NPs of ≈50 nm in diameter over a large area on a Si substrate using an improved variant of the drop-casting method. The formation of a monolayer is significantly influenced by the NPs concentration, the stearyl alcohol concentration, the volume of the droplet, and the annealing time. The main idea in the present study is the addition of stearyl alcohol to the NP dispersion from where the monolayers are formed. The stearyl alcohol results in monolayers with improved order, as confirmed with SEM for the local order and GISAXS for the long-range hexagonal order. A heat treatment melting the stearyl alcohol in the monolayers leads to nearly perfectly ordered monolayers. This improved ordering is a result of giving the NPs more time to further self-assemble, which is then followed by solidifying the monolayer by simple cooling to room temperature, preventing the large volume change as obtained after evaporation of a solvent. We propose that the heat treatment in combination with a compatible additive with melting point significantly below that of the particles, can be a general method to improve the ordering between particles in monolayers as well as multilayers.

Conflicts of interest

There are no conflicts to declare.

Acknowledgements

This work was funded in part by the Brain Gain Fund of Forschungszentrum Jülich GmbH. We thank Jochen Friedrich (PGI-7) for the opportunity to use their SEM and for technical support.

Notes and references

1 M. A. Boles, M. Engel and D. V. Talapin, *Chem. Rev.*, 2016, **116**, 11220–11289.
2 V. Karol, *et al.*, *Nanotechnology*, 2012, **23**, 045101–045705.
3 C. B. Murray, C. R. Kagan and M. G. Bawendi, *Annu. Rev. Mater. Sci.*, 2000, **30**, 545–610.
4 T. Ogi, L. B. Modesto-Lope, F. Iskandar and K. Okuyama, *Colloids Surf., A*, 2007, **297**, 71–78.
5 S. Shinde, S. Park and J. Shin, *J. Semicond.*, 2015, **36**, 043002.
6 M. Szekeres, O. Kamalin, R. A. Schoonheydt, K. Wostyn, K. Clays, A. Persoons and I. Dékány, *J. Mater. Chem.*, 2002, **12**, 3268–3274.
7 T. Okubo, S. Chuj, S. Maenosono and Y. Yamaguchi, *J. Nanopart. Res.*, 2003, **5**, 111–117.
8 Y. Wang, Y. L. Chen, H. Yang, H. Q. Guo, W. Zhou and M. Tao, *J. Mater. Sci.*, 2010, **28**, 467–478.
9 H. B. Bohidar and K. Rawat, *Design of Nanostructures: Self-Assembly of Nanomaterials*, Wiley-VCH Verlag GmbH & Co. KGaA, 1st edn, 2017.
10 F. J. Arriagada and K. Osseo-Asare, *J. Colloid Interface Sci.*, 1999, **211**, 210–220.
11 F. J. Arriagada and K. Osseo-Asare, *Colloids Surf.*, 1992, **69**, 105–115.
12 K. Osseo-Asare and F. J. Arriagada, *Colloids Surf.*, 1990, **50**, 321–339.
13 A. K. van Helden, J. W. Jansen and A. Vrij, *J. Colloid Interface Sci.*, 1981, **81**, 354–368.
14 J. Kohlbrecher, J. Buitenhuis, G. Meier and M. P. Lettinga, *J. Chem. Phys.*, 2006, **125**, 44715.
15 Jülich Centre for Neutron Science, *Journal of Large-Scale Research Facilities*, 2016, **2**, A61, DOI: 10.17815/jlsrf-2-109.
16 M. Hu, S. Chujo, H. Nishikawa, Y. Yamaguchi and T. Okubo, *J. Nanopart. Res.*, 2004, **6**, 479–487.
17 E. Josten, E. Wetterskog, A. Glavic, P. Boesecke, A. Feoktystov, E. B. Reuters, U. Rücker, G. Salazar-Alvarez, T. Brückel and L. Bergström, *scientific reports*, 2017, **7**, 2802.
18 G. Renaud, R. Lazzari and F. Leroy, *Surf. Sci. Rep.*, 2009, **64**, 255–380.
19 J. Nielsen and D. Morrow, *Elements of Modern X-ray Physics*, John Wiley & Sons, 2001.
20 S. Disch, E. Wetterskog, R. P. Hermann, G. Salazar-Alvarez, P. Busch, T. Brückel and L. S. K. Bergström, *J. Nanosci. Lett.*, 2011, **11**, 1651–1656.
21 D. Mishra, *et al.*, *Nanotechnology*, 2012, **23**, 055707.
22 G. Pospelov, W. Van Herck, J. Burle, J. M. Carmona Loaiza, C. Durniak, J. M. Fisher, M. Ganeva, D. Yurov and J. Wuttke, *J. Appl. Crystallogr.*, 2020, **53**, 1600–5767.